A debubbler for microfluidics utilizing air-liquid interfaces

Daming Cheng and Hongrui Jiang[a)]
Materials Science Program, University of Wisconsin—Madison, 1415 Engineering Drive, Madison, Wisconsin 53706, USA

(Received 15 July 2009; accepted 21 October 2009; published online 25 November 2009)

We present a debubbler for the removal of air bubbles in aqueous liquids in microfluidics. The debubbler is realized through an array of cylinder-shaped air-liquid interfaces, or air-pillars, formed directly into the microfluidic channels by surface tension. The debubbler demonstrated effective trapping and removal of both chemically generated bubbles (several nanoliters to several microliters in volume) and air slugs with several microliters in volume, which were formed by high infusion rates of bubble series introduced into the microchannel. © *2009 American Institute of Physics*. [doi:10.1063/1.3263944]

Inadvertently introduced and unwanted bubbles in microfluidic networks could negatively and significantly affect the performance of the device as well as the experimental results.[1,2] There are thus high demands from both biomedical instrument industries and biochemical assay laboratory researches for a bubble controlling method or device. Some methods and devices have recently been developed for this purpose that demonstrated capabilities of trapping or removing air bubbles in microfluidic channels.[3–6] However, devices with high bubble-removing capacity and speed, which can be conveniently incorporated with regular microfluidic operations, are still sought.

We present here a practical passive debubbler for highly efficient air bubble removal from aqueous liquids in microfluidic channels by leveraging the advantages of controlled liquid-air interfaces[7,8] and the physics of air bubble aggregation in water.[9] The debubbler demonstrated the capability of removing various kinds of bubbles, from chemically generated bubbles with volumes of several nanoliters (nL) to larger air slugs (bubbles that fill the channel and touch the sidewalls, and with volume about or larger than 1 μL) injected into the microchannel. The liquid flow does not need to be kept stagnant (i.e., flow can be maintained) during the bubble removal process. This debubbler also demonstrates high speed of bubble removal, zero power consumption, robustness, and reusability, and relatively simple structures which permit high-throughput industrial production.

The device was designed based on the physics of the bubble aggregation in aqueous liquid. Two spherical air bubbles in the proximity of each other in aqueous solutions with radii of r_1 and r_2, respectively, tend to aggregate into a bigger bubble to minimize the total surface energy. It can be shown that

$$E_{s,1} = \gamma \cdot 4\pi R^2 < \gamma \cdot 4\pi(r_1^2 + r_2^2) = E_{s,0},$$

where $E_{s,0}$ and $E_{s,1}$ are the total surface energy of the two original air bubbles and the surface energy of the combined air bubble, respectively, and R is the radius of the combined bubble.

In addition, from the perspective of molecular interactions, when two air bubbles approach each other, a thin film of water sandwiched between the two air phases forms, as shown in the top-view inset in Fig. 1(a). The attractive van der Waals force between the two air phases induces thinning of the water film. Under this force, the water film breaks and the two air phases merge.[9] Inspired by this phenomenon, it is conceivable that we may utilize liquid-air interfaces, such as a vertical air-water interface at a hydrophilic-hydrophobic boundary (H-H boundary) in a microfluidic channel,[8] so that the air bubble would merge into the air phase across the interface and be removed from the liquid phase.

Therefore, a debubbler chamber containing several cylinder-shaped air-liquid interfaces, or air pillars, was designed and integrated into a microfluidic channel network. Figure 1(a) illustrates the design of the debubbler. A polystyrene plate was used as the top of the microfluidic channels. An array of through holes (~2 mm in diameter) was drilled in the top plate. In this letter, the air pillar design has been improved from our previous letter[10] by introducing a circular H-H boundary on the bottom surface of the channel, aligned with the orifice on the top surface, as shown in Fig. 1. The

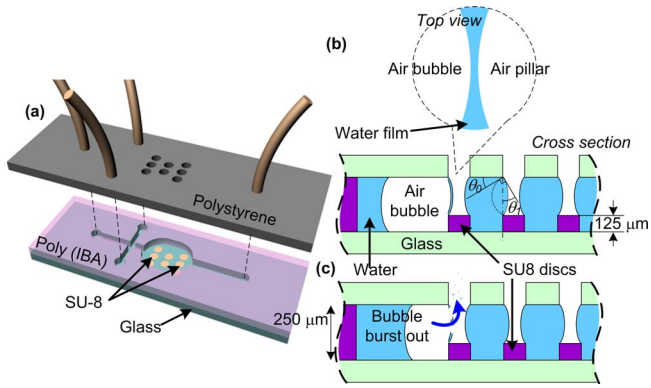

FIG. 1. (Color online) (a) Schematic of the debubbler: a microfluidic channel network with three inlets and an outlet and a debubbler chamber with pairing holes and hydrophobic pads for air pillar formation. (b) A cross section of the debubbler illustrating the operational principle of the device. Air pillars are formed between the aligned holes and the SU-8 disks. Water and an air bubble are introduced from the upstream (left hand side) of the channel. The top-view inset shows that a water thin film is formed between the air bubble and the air pillar. (c) The water thin film breaks, and the bubble merges into the air pillar and is vented out of the channel.

[a)]Author to whom correspondence should be addressed. Electronic mail: hongrui@engr.wisc.edu. Tel.: 608-265-9418. FAX: 608-262-1267. Present address: Department of Electrical and Computer Engineering, University of Wisconsin—Madison, 1415 Engineering Drive, Madison, WI 53706, USA.

H-H boundaries were formed by patterning disk-shaped structures made of a hydrophobic photoresist, SU-8, on the surface of the hydrophilic glass bottom substrate. The diameter of these disk-shaped structures was 2 mm, and the thickness was 150 ± 15 μm. The channel structure with a height of 250 μm was constructed with photosensitive polymer, poly isobornyl acrylate using liquid phase photopolymerization (LP^3) process.[11–13] Ethyl vinyl acetate microbore tubings were plugged into the three inlet holes and one outlet hole and sealed with epoxy glue. The detailed fabrication process is described in the supplementary material (see Ref. 14, which also includes two video clips that show the structure of the debubblers and their operations).

Air pillars would form beneath the holes when the channel is filled with aqueous liquid, due to the pinning effect of the surface tension at the 90° edge of the orifices on the top surface, and the H-H boundary at the bottom. As shown in Fig. 1(b), the area between the two dashed-line curves represents the range in which the meniscus can be sustained. Therefore, when the water-air interface contact line with the top surface reaches the orifice,[10] it will maintain its position with only the contact angle of the meniscus changing from θ_0 to $90° + \theta_1$, where θ_0 and θ_1 are the water contact angles on the top surface and side wall of the holes, respectively. According to Young–Laplace relation, this range of angle corresponds to a certain range of pressure that the meniscus can sustain. As a result, the interface is pinned at the orifice, while the water pressure in the channel can vary in a corresponding range. The interface structures were more robust to endure higher pressures in the channel during operation, compared to the structure without the hydrophobic disks at the bottom.[10] The maximum pressure that can be sustained by an air pillar is inversely proportional to the height of the air pillar. The 150-μm hydrophobic disks elevated the bottom of the air pillars to be closer to the top surface. Therefore, the maximum sustainable pressure is increased, while the height of the channel can be designed as 250 μm for a higher liquid flow rate.

The formation and the sustainability of the air pillars, i.e., cylinder-shaped liquid-air interfaces, were first tested. Deionized (DI) water (with blue food dye for better visualization) was first introduced into the channel through the liquid inlet from a 1 mL plastic syringe (BD medical Inc., Nogales, AZ, USA), which was controlled by a programmable syringe pump (Cole-Parmer, Vernon Hills, IL, USA). The operation was observed using a stereomicroscope (Nikon SMZ1500, Nikon Instruments, Inc., Melville, NY, USA) and recorded with a charge-coupled device camera at a rate of 33.3 frames per second. Infusion rate up to 60 μL/min (correspondingly, velocity of 48 mm/min) was sustained by the eight air pillars formed. When infusion rate was raised higher than 60 μL/min, the liquid-air interface at the weakest (due to slight misalignment resulting in reduced surface area) air pillar started to break.

Bubbles were artificially generated in two mechanisms, chemical reaction and air bubbles introduced from upstream, which are commonly encountered situations in microfluidic and biomedical devices.

To generate bubbles through a chemical reaction, a crossing channel structure was created in front of the chamber. Saturated sodium bicarbonate ($NaHCO_3$) solution (10 w% at 20 °C) and 1 w% hydrochloric acid (HCl) solution

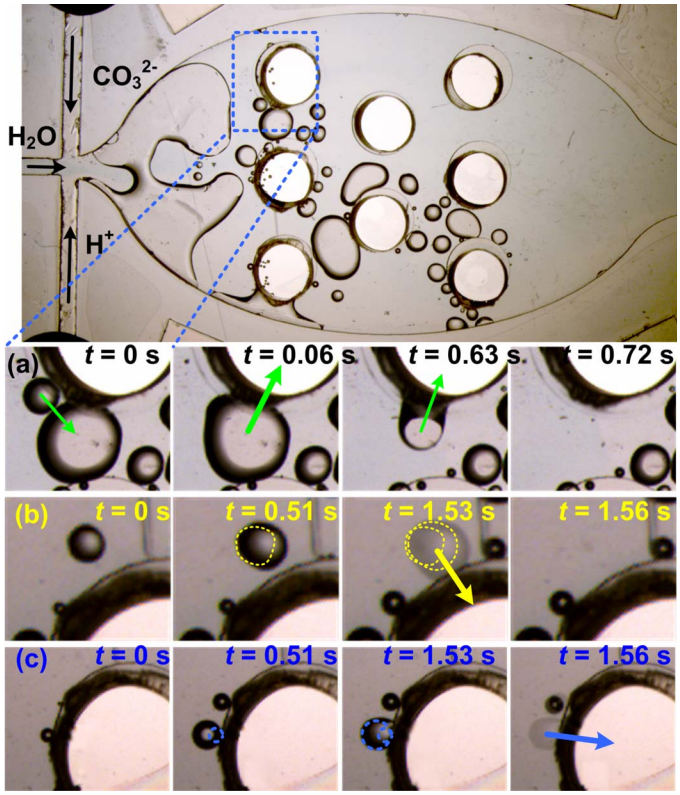

FIG. 2. (Color online) Frames captured from a video showing the debubbler removing chemically generated CO_2 gas. The CO_2 bubbles were observed to be trapped and vented via three scenarios: (a) Small CO_2 bubble merges into a bigger bubble, and the merged bubble is trapped and vented by an air pillar; (b) a bubble nucleates in the proximity of an air pillar, grows until it contacts an air pillar and exits the chamber; (c) bubbles nucleate at the edges of the SU-8 disks and are vented out shortly by the air pillar.

were introduced through the upper and lower vertical channel, respectively, as shown in Fig. 2. The mixed streams flowed into the chamber and carbon dioxide (CO_2) was generated in it. DI water dyed blue was introduced from the horizontal channel in order to drive the CO_2 bubble to the downstream when the flow rates of reacting fluids were lower, such as 5 μL/min. In the chamber, the CO_2 bubbles were observed to nucleate, grow, and be trapped and vented out of the channel. In detail, three scenarios of debubbling were observed and shown in Fig. 2(a)–2(c). In the first scenario [Fig. 2(a)], a smaller CO_2 bubble (approximately 7.8 nL) was generated (at the tail of the arrow at $t=0$ s), and merged into a bigger bubble ($t=0.06$ s). The latter then merged into the air pillar and was vented out of the channel ($t=0.06$ s through $t=0.72$ s). In the second scenario [Fig. 2(b)], a bubble nucleated in the proximity of an air pillar, grew until it contacted the air pillar and exited the chamber through the air pillar. The edge of the SU-8 disks at the bottom substrate of the air pillar often served as nucleation sites for the generation of the CO_2 bubbles. The bubbles generated at these locations were shortly vented out by the air pillar, as shown in Fig. 2(c) as the third scenario. The bubble removal cycles were conducted repetitively, constantly demonstrating the removal of air bubbles with volumes ranging from several nL to several μL (Fig. 3; also see Ref. 14). The capacity of removing chemically generated bubbles was tested by increasing the infusion rate of the reacting fluids. When the infusion rate of DI water, $NaHCO_3$ solution, and HCl solution were 0, 20, and 20 μL/min, re-

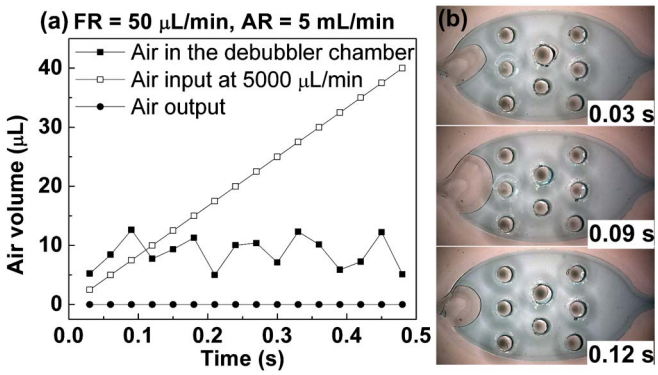

FIG. 3. (Color online) The debubbler removes the air bubbles in a coflow with liquid from upstream. DI water was input from the upstream at a flow rate of 50 μL/min, and air was input at a rate of AR=5 mL/min. (a) The volume of input air increased linearly along the time; the air volume in the chamber demonstrated a fluctuation; the volume of the air downstream of the debubbler remained zero. The data shown are representative; only 0.5 s is shown here for better visualization of the detail. (b) A sequence of photographs showing the bubble removal process. When the air slug contacts one air pillar, the air is vented through the air pillar, and then the surface tension forces the air pillar to snap back and recover.

spectively, which corresponded to a CO_2 generation rate of 134 μL/min, the maximum CO_2 bubble removing capacity was reached.

The debubbler was also tested to remove the air bubbles in a coflow with liquid from upstream. DI water was introduced through the debubbler at a flow rate of 50 μL/min, and eight air pillars were formed. Air was then introduced by a syringe through one of the inlet at the upstream at an initial infusion rate of 10 μL/min. Series of air bubbles were formed by the liquid-air coflow. The bubbles were trapped and vented by the air pillars, and the downstream of the debubbler was kept air-free. The infusion rate of air was increased to 5000 μL/min, when the limit of the bubble removal was reached. Figure 3 demonstrates the bubble trapping and venting process in this test. The volumes of input air, bubble in the chamber, and input DI water, evolving with time, were calculated from the video frames and shown in Fig. 3(a) (also see Ref. 14). As shown in Fig. 3(b), in one cycle of the removing process, when the air bubble (or slugs) contacted one of the air pillars, the air would be vented through the air pillar, and then the surface tension forced the air pillar to snap back and recover.

In our experiment, the device showed good robustness and reusability; it was tested more than one hundred times without visible degradation. Each test lasted until the supply ran out. It should be noted that if a bubble is generated and remains far from the air pillars, it cannot be trapped and vented by the air pillars. As laminar flows are dominant in microchannels, bubbles will flow along smooth streamlines. Bubbles traversing streamlines between air pillars will pass through the debubbler without removal. The fact that bubbles significantly smaller than the air pillar separation may not be captured must inform design.

In summary, we have demonstrated a debubbler, a bubble removal device integrated in a microfluidic network. An array of air-pillar structures formed through surface tension held air-liquid interfaces were used to remove unwanted air bubbles from the microchannel and kept the downstream bubble-free. The device was able to remove chemically generated CO_2 bubbles (each of nL to μL in volume) from the channel. It also demonstrated removal of large-volume air slugs introduced from upstream at a maximum rate of 5 mL/min. In both cases, the downstream of the debubbler chamber was kept free of the bubbles from upstream.

The debubbler does not require additional peripheral equipment nor consumes power. The device also demonstrates good robustness and reusability in repeated operations. The relatively simple structure of the device makes high-throughput industrial production possible. However, care must be taken in the alignment step, as we observed weakening of air pillar pinning due to reduction in the pinned surface. In future work, we will perform simulation to analyze the operation of the debubbler, determine the velocity and pressure distribution in the chamber with given infusion rate, and find the optimal size, density, and number of the air pillars. Assembling method could be improved too for better alignment of the hole-disk pairs.

This research was partly supported by U.S. National Science Foundation (Grant No. ECCS 0622202) and partly by U.S. Army Medical Research and Acquisition Activity (Award No. W81XWH 07-2-0045) through a subcontract from BioSentinel Pharma LLC. The authors would like to thank Dr. Xuefeng Zeng, Chi-wei Lo, Difeng Zhu, and David Busacker for insightful discussions over fabrication methods and theoretical calculation.

[1]R. H. Liu, Q. Yu, and D. J. Beebe, J. Microelectromech. Syst. **11**, 45 (2002).
[2]E. Leclerc, Y. Sakai, and T. Fujii, Biomed. Microdevices **5**, 109 (2003).
[3]J. H. Kang, Y. C. Kim, and J. K. Park, Lab Chip **8**, 176 (2008).
[4]D. T. Eddington, "Chips & Tips: In-line microfluidic bubble trap," Lab Chip (2006). http://www.rsc.org/Publishing/Journals/lc/bubble_trap.asp.
[5]A. M. Skelley and J. Voldman, Lab Chip **8**, 1733 (2008).
[6]J. H. Sung and M. L. Shuler, Biomed. Microdevices **11**, 731 (2009).
[7]J. Atencia and D. J. Beebe, Nature (London) **437**, 648 (2005).
[8]D. M. Cheng, Y. J. P. Choe, and H. R. Jiang, J. Microelectromech. Syst. **17**, 962 (2008).
[9]J. N. Israelachvili, *Intermolecular and surface forces*, 2nd ed. (Academic, London, 1991), p. 450.
[10]J. Greenwood, D. M. Cheng, Y. Liu, and H. R. Jiang, *Proceedings of the IEEE Sensors Conference* (2008), pp. 720–723.
[11]A. K. Agarwal, D. J. Beebe, and H. R. Jiang, J. Micromech. Microeng. **16**, 332 (2006).
[12]A. K. Agarwal, S. S. Sridharamurthy, D. J. Beebe, and H. R. Jiang, J. Microelectromech. Syst. **14**, 1409 (2005).
[13]D. J. Beebe, J. S. Moore, Q. Yu, R. H. Liu, M. L. Kraft, B. H. Jo, and C. Devadoss, Proc. Natl. Acad. Sci. U.S.A. **97**, 13488 (2000).
[14]See EPAPS supplementary material at http://dx.doi.org/10.1063/1.3263944 for the detailed fabrication process and videos showing the operations of the debubbler.